Turkish Journal of Chemistry

http://journals.tubitak.gov.tr/chem/

Research Article

Turk J Chem
(2019) 43: 766 – 777
© TÜBİTAK
doi:10.3906/kim-1809-56

Tribological behavior and quantum chemical calculations of protic ionic liquids: synthesis, spectroscopic, and thermal properties

Ahmet KARADAĞ[1,2,*], **Hüseyin AKBAŞ**[2], **Duran KARAKAŞ**[3], **Kadir Cihan TEKİN**[4], **Erdem KORKMAZER**[2]

[1]Department of Biotechnology, Faculty of Sciences, Bartın University, Bartın, Turkey
[2]Department of Chemistry, Faculty of Science and Letters, Gaziosmanpaşa University, Tokat, Turkey
[3]Department of Chemistry, Faculty of Science, Cumhuriyet University, Sivas, Turkey
[4]Department of Metallurgical and Materials Engineering, Faculty of Engineering, Dokuz Eylül University, İzmir, Turkey

Received: 26.09.2018 • **Accepted/Published Online:** 27.02.2019 • **Final Version:** 11.06.2019

Abstract: Protic ionic liquids (PILs) were synthesized through a stoichiometric neutralization reaction between 2,2′-(ethylenedioxy)-bis(ethylamine) { Edbea} and various acids (formic, acetic, boric, decanoic, and gentisic acid). The PILs were characterized by elemental analyses, FTIR, ^{1}H and ^{13}C NMR spectroscopy, and thermogravimetric analysis. All the PILs except **PIL3** were liquid at room temperature. The viscosity of the PILs (**PIL1**, **2**, **4**, **5**) was measured using a cone-and-plate viscometer at ambient temperature. Quantum chemical calculations were used to explain the cation/anion ratio in the PILs. Reaction energies in the gas phase calculated at M062X/6-311+G(d,p) level were used to determine the cation/anion ratio. A sliding wear test was conducted at room temperature using an AA7075 disc specimen against a stationary 100Cr6 steel ball. The wear protection of PILs and 15W40 engine oil was determined by considering the volume loss of AA7075.

Key words: Protic ionic liquid, tribology, spectroscopy, quantum chemical calculation

1. Introduction

Ionic liquids (ILs) are compounds that consist wholly of ions and remain liquid below 100 °C.[1] Generally, ILs are composed of bulky organic cations paired with organic or inorganic anions bound together by electrostatic interactions and they have unique physical properties such as negligible vapor pressure, high thermal stability, nonflammability, a wide electrochemical window, and a wide fluid range.[2] ILs can be classified into two broad categories: protic ILs (PILs) and aprotic ILs (APILs). Compared to APILs, PILs often have higher conductivity and fluidity and lower melting points.[3] PILs are an important subgroup of ionic liquids readily obtained by stoichiometric reaction of Brønsted acids and Brønsted bases.[4] The most important property that distinguishes PILs from other ILs is the proton transfer from the acid to the bases, which leads to the presence of proton donor and proton acceptor sites that can be used to form a network of hydrogen bonds.[5,6] The most extensively studied PILs have advantageous properties such as low cost, easy preparation, and varying proton activity.[7] The first PIL, ethanolammonium nitrate (mp 52–55 °C), was reported by Gabriel in 1888.[8] Ethylammonium nitrate (mp 12.5 °C), the first known room temperature IL, was reported by Walden in 1914 and attracted more

*Correspondence: ahmet.karadag@gop.edu.tr

This work is licensed under a Creative Commons Attribution 4.0 International License.

attention than ethanolammonium nitrate. Due to its similar properties to water, it is distinguished from other ILs and many other solvents.[9]

The different potential applications of ILs depend on the physicochemical properties, which vary depending on the cation and anion structures used. ILs are widely used as catalysts in organic reactions,[10] metal ion separations,[11] as pharmaceutical solvent for drugs,[12] in electrochemical devices,[13] for removal of pollutants,[14] and the like. Recently, a new class of high-molecular-weight precursors, phosphazene-based protic ionic liquids (PzPILs), have also been investigated for their antiproliferative effects.[15–19]

Currently, quantum chemical calculations are widely used to explain experimental observations, molecular energies, molecular structures, reaction energies, molecular orbitals, atomic charges, molecular spectra (IR, NMR), polarizabilities, and thermochemical properties.[20–24]

Application of ILs as lubricants has also been the focus of several recent studies owing to their distinct properties such as extremely low vapor pressure, high thermal stability, low flammability, and inherent polarity.[25] Based on these properties, ILs can be utilized in high temperature environments, reduced pressure environments, and microelectromechanical systems, for which conventional lubricants do not function efficiently or fail to function. ILs are also used as lubricant additives to improve the frictional properties of lubricants.[26,27] ILs can acquire various characteristics by selecting different combinations of anions and cations; therefore, it is important to choose a suitable IL for a specific application. There are many studies on the lubrication of aluminum and steel with various ILs including different anions and cations.[28–36]

In the present study, PILs consisting of 2-(2-(2-aminoethoxy) ethoxy)ethanaminium cation and anions of different acids were obtained, namely 2-(2-(2-aminoethoxy)ethoxy)ethanaminium formate (**PIL1**), 2-(2-(2-aminoethoxy)ethoxy) ethanaminium acetate (**PIL2**), 2-(2-(2-aminoethoxy)ethoxy) ethanaminium dihydrogenborate (**PIL3**), 2-(2-(2-aminoethoxy)ethoxy)ethanaminium decanoate (**PIL4**), and 2-(2-(2-aminoethoxy) ethoxy)ethanaminium 2,5-dihydroxybenzoate (**PIL5**) (Scheme). The structure of the synthesized PILs was determined by elemental analyses, FTIR, and ^{1}H and ^{13}C NMR techniques. Quantum chemical calculations were used to explain the cation/anion ratio in the PILs. In the calculations, we used the density functional theory hybrid method M062X and 6-311+G (d,p) basis set with high angular momentum for representing atomic orbitals. The frictional and wear properties of the PILs and 15W40 engine oil were evaluated using sliding wear tests, which were conducted at room temperature using an AA7075 disc specimen against a stationary 100Cr6 steel ball. The wear performance of PILs and 15W40 engine oil was determined by considering the volume loss of AA7075.

2. Results and discussion

2.1. Syntheses and structural characterization

PILs **1**–**5** were prepared for the reactions of 2,2′-(ethylenedioxy)-bis(ethylamine) { Edbea} with formic, acetic, boric, decanoic, and gentisic acid in the molar ratio 1:1 (Scheme). PILs **1**, **2**, **4**, and **5** are liquid state and **PIL3** is in a creamy state at room temperature (Supplementary Information, Figure S1). Data obtained from the microanalyses, and FTIR, ^{1}H, and ^{13}C{ ^{1}H} NMR data were consistent with the proposed structures of the PILs. The elemental analysis results indicate that PILs **1**–**3** are diprotonated with the nitrogen of amine, but PILs **4** and **5** are monoprotonated with the nitrogen of amine. These structures were supported by quantum chemical calculations.

The chemical shifts, multiplicities, and the coupling constants are very useful for interpretation of the ^{1}H

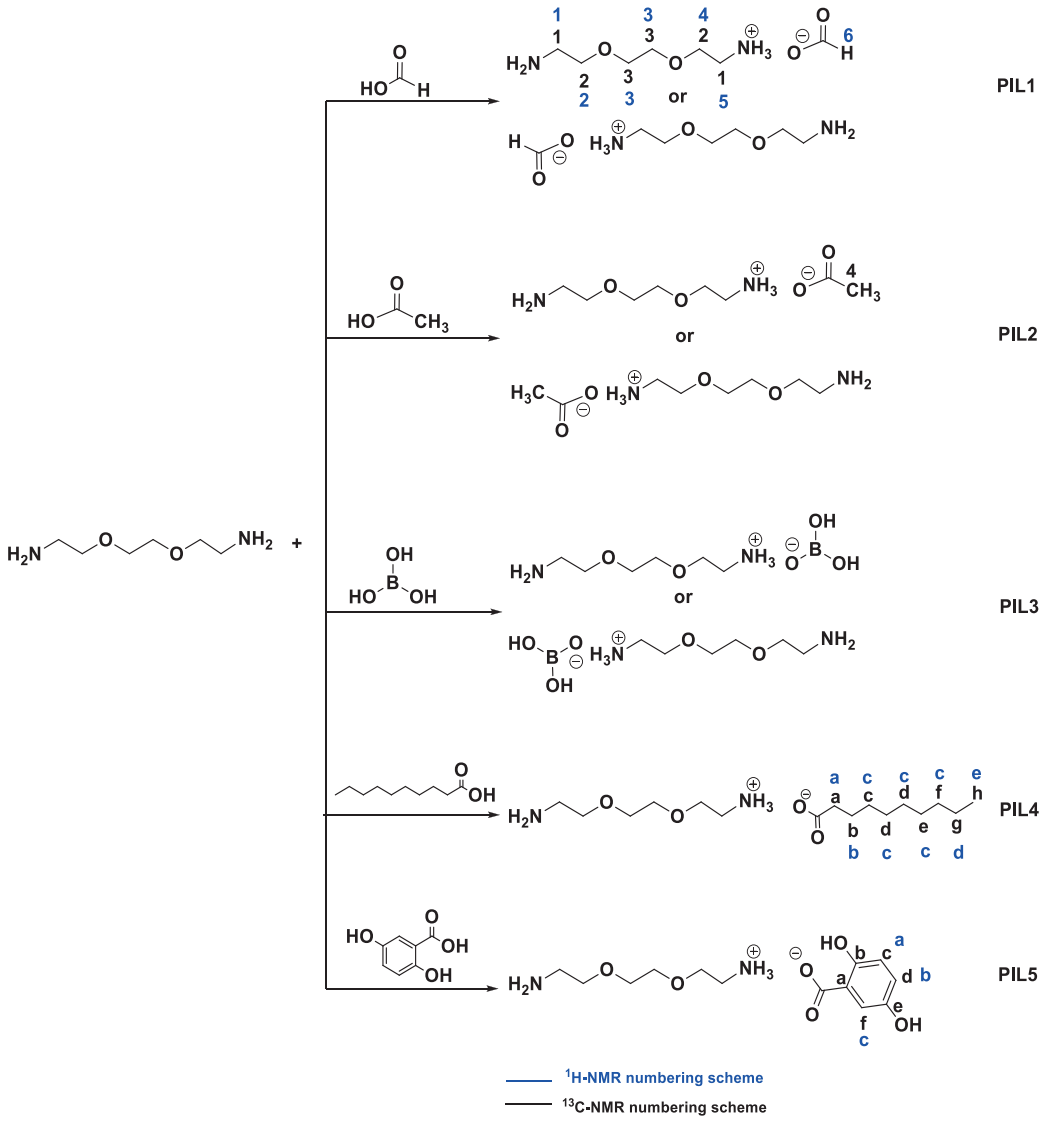

Scheme. The scheme represents the novel PILs.

and ^{13}C{ ^{1}H} NMR signals of all the PILs (Supplementary Information, Figures S2–S11). The amine C$\boldsymbol{H_2}$ protons for all compounds were observed at about 2.75 ($\boldsymbol{H_1}$), 3.50 ($\boldsymbol{H_2}$), 3.38 ($\boldsymbol{H_3}$), 4.31 ($\boldsymbol{H_4}$), and 3.06 ($\boldsymbol{H_5}$) ppm, respectively. The amine N$\boldsymbol{H_2}$ protons for all compounds were observed at about 5.64 ppm and N$\boldsymbol{H_3^+}$ protons were observed at about 8.06 ppm. In the ^{13}C{ ^{1}H} NMR spectra of PILs **1**, **2**, **4**, and **5**, the carbonyl carbon atoms ($\boldsymbol{C}$=O) were observed at 167.11, 176.22, 176.95, and 172.40 ppm, respectively. The amine $\boldsymbol{C}$H$_2$ carbons for all compounds were observed at about 41.96 ($\boldsymbol{C_1}$), 70.68 ($\boldsymbol{C_2}$), and 69.66 ($\boldsymbol{C_3}$) ppm, respectively.

The obtained characteristic absorption bands of PILs **1**–**5** in the range of 2703–2697 cm^{-1} are attributed to the $\nu^{+}_{(NH)}$ stretching vibrations for the PILs (Supplementary Information, Figure S12). PILs **1**, **2**, **4**, and **5** show two strong absorption bands at 1587–1565 and 1491–1473 cm^{-1}, which are assigned to the asymmetric and symmetric stretching vibrations of the ν_{COO-} bonds, respectively, clearly indicating PIL formation.

2.2. Quantum chemical calculations

In order to explain the cation/anion ratio of the PILs, cations (C), anions (A), and PILs (CA and CA_2) were optimized at M062X/6-311+G(d,p) level in the gas phase. The optimized structures of cations (C) and anions (A) are given in Figure S13 (Supplementary Information) and the optimized structures of CA- and CA_2-type PILs are shown in Figures 1 and 2, respectively.

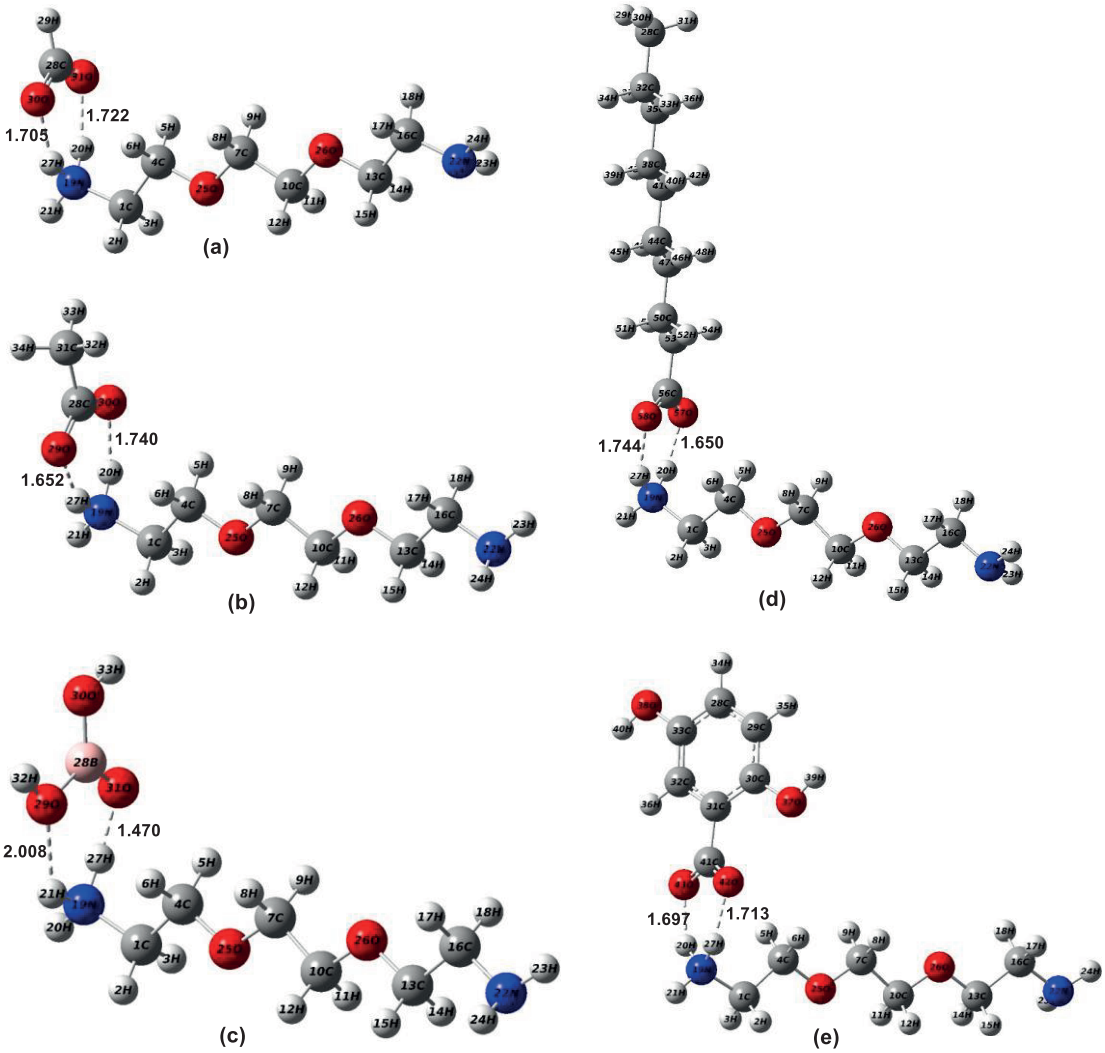

Figure 1. Optimized structures of CA-type ILs obtained at the M062X/6-311+G(d,p) level in the gas phase. (a) [EdbeaH][HCOO], (b) [EdbeaH][CH_3COO], (c) [EdbeaH] [H_2BO_3], (d) [EdbeaH][$CH_3(CH_2)_8COO$], (e) [EdbeaH][$C_6H_3(OH)_2COO$].

As shown in Figures 1 and 2, the interaction between the cation and the anion is provided by the formation of hydrogen bonds. It can be considered that two hydrogen bonds are formed in CA-type ILs and four hydrogen bonds are formed in CA_2-type ILs. Hydrogen bond lengths are shown in Figures 1 and 2. Figures 1 and 2 show that the calculated hydrogen bond lengths vary between 1.5 and 2.0. These hydrogen bonds are expected to provide sufficient energy to form an IL. For this reason, the reaction energies of CA- and CA_2-type PILs were calculated and these are shown in Table 1.

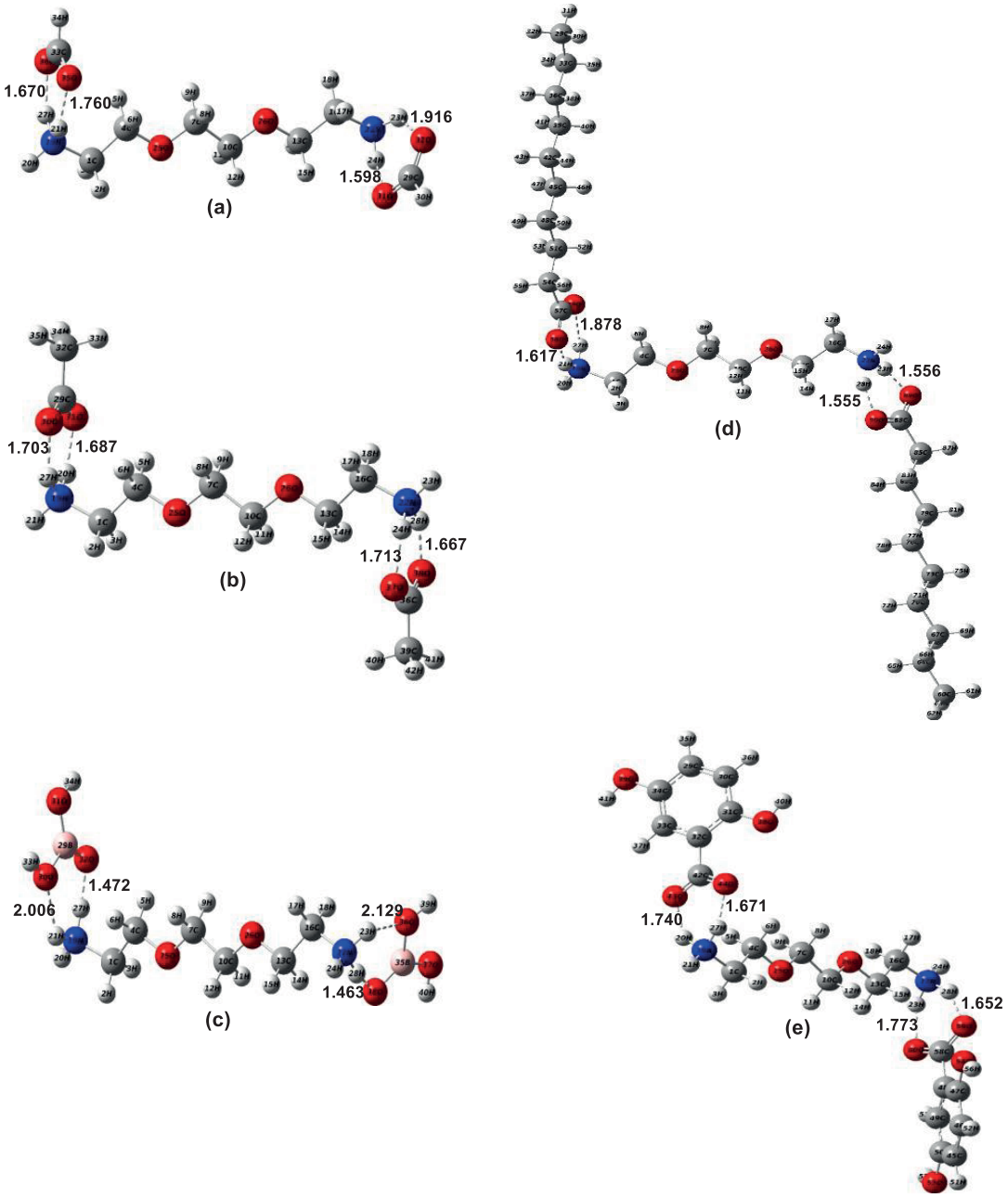

Figure 2. Optimized structures of CA_2-type ILs obtained at the M062X/6-311+G(d,p) level in the gas phase. (a) $[EdbeaH_2][HCOO]_2$, (b) $[EdbeaH_2][CH_3COO]_2$, (c) $[EdbeaH_2][H_2BO_3]_2$, (d) $[EdbeaH_2][CH_3(CH_2)_8COO]_2$, (e) $[EdbeaH_2][C_6H_3(OH)_2COO]_2$.

The reaction energies (ΔE) of CA- and CA_2-type ILs are exothermic. In addition, the reaction energies of the CA_2-type ILs are two times lower than those of the CA-type ILs. These results show that the formation of CA_2-type ILs is more desirable than that of CA-type ILs. According to the elemental analysis results, $[EdbeaH_2][HCOO]_2$, $[EdbeaH_2][CH_3COO]_2$, $[EdbeaH_2][H_2BO_3]_2$ [EdbeaH] $[CH_3(CH_2)_8COO]$, and $[EdbeaH][C_6H_3(OH)_2COO]$ ILs were synthesized in this work. The last two are of CA type. Experimentally, the formation of the CA-type ILs can be attributed to the phase, entropy, and solvent effects.

Table 1. Reaction energies of PILs of type CA and CA_2.

PILs	E_{PIL} (a.u.)	E_C (a.u.)	E_A (a.u.)	ΔE (a.u.)
[EdbeaH][HCOO]	–687.571025	–498.196081	–189.167934	–0.20701
$[EdbeaH_2][HCOO]_2$	–877.281199	–498.472555	–189.167934	–0.47278
$[EdbeaH][CH_3COO]$	–726.853704	–498.196081	–228.448690	–0.20893
$[EdbeaH_2][CH_3COO]_2$	–955.849632	–498.472555	–228.448690	–0.47970
$[EdbeaH][H_2BO_3]$	–750.274469	–498.196081	–251.862080	–0.21631
$[EdbeaH_2][H_2BO_3]_2$	–1002.688721	–498.472555	–251.862080	–0.49201
$[EdbeaH][CH_3(CH_2)_8COO]$	–1041.041939	–498.196081	–542.638261	–0.20760
$[EdbeaH_2][CH_3(CH_2)_8COO]_2$	–1585.079800	–498.472555	–542.638261	–0.46783
$[EdbeaH][C_6H_3(OH)_2COO]$	–1068.937200	–498.196081	–570.539250	–0.20187
$[EdbeaH_2][C_6H_3(OH)_2COO]_2$	–1640.014162	–498.472555	–570.539250	–0.46311

2.3. Thermal studies

The thermogravimetric analyses (TGA) of PILs **1**–**5** were performed in the temperature range of 35–500 °C under a nitrogen atmosphere at the heating rate of 10 °C/min. TG and DTG curves of PILs **1**–**5** are shown in Figure 3 and Figure S14 (Supplementary Information), and the thermoanalytical data of these compounds are summarized in Table S1 (Supplementary Information). In the first step, adsorbed water was removed from PILs **1**, **2**, **4**, and **5**, while ethanol was removed from **PIL3**. The thermal decomposition of PILs **1**–**5** starts with the decomposition of formate, which is followed by acetate, borate, decanoate, and 2,5-dihydroxy benzoate anions, in that order. Afterwards, the 2,2′-(ethylenedioxy)-bis(ethylaminium) cation starts to decompose. The thermal decomposition of PILs **1**, **2**, and **4** is completely finished at about 500 °C, but the decomposition process for PILs **1** and **5** is not completed at this temperature, with residue of about 15.70% and 6.22%, respectively (Supplementary Information, Table S1).

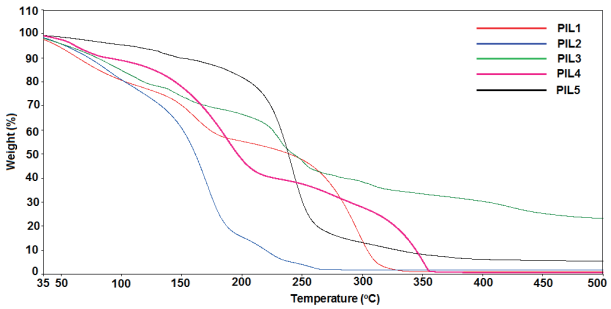

Figure 3. TGA curves of PILs **1**–**5**.

2.4. Viscosity

With the exception of **PIL3**, which is a liquid, these ILs had viscosities between 42.3 and 5239.0 cP at about 30 °C (Table 2). At a particular temperature, the viscosity of the linear PILs (**PIL2** and **PIL4**) increased with increasing anion chain length. It was observed that **PIL5**, having an aromatic anion, had the highest viscosity.

Table 2. Viscosities of PILs **1**–**5**.

Compound	Viscosity (cP)	Speed (RPM)	Torque (%)	Temperature (°C)	Spindle
PIL1	160.8	11	54.1	27.2	CP-40
PIL2	42.3	39	50.4	30.4	CP-40
PIL4	508.2	98	50.2	30.8	CP-52
PIL5	5239.0	10	52.8	30.8	CP-52

2.5. Tribology studies

The mean coefficient of friction (COF) values recorded during the sliding wear test are shown in Figure 4. The 15W40 engine oil showed almost stable and low COF throughout the wear test since this commercial engine oil has been developed to meet the demands for tribological applications. In the case of **PIL1**, there are many upward spikes in COF values, which are related to temporary loss of the lubricating layer from the steel/aluminum interface, causing metal to metal contact. In the cases of **PIL2** and **PIL3**, COF increased to higher values compared to the other lubricants at the beginning of the wear test then slightly decreased. The increased COF value indicates the establishment of metal to metal contact, which can cause adhesive wear of rubbing counterfaces. **PIL4** exhibited the lowest COF, which is indicative of formation of a stable lubricant layer separating the steel ball from the aluminum disc. The COF of **PIL5** showed a slight and a constant increase with increasing test period, which can be ascribed to the increased viscosity of IL.

The wear profiles and wear rates of the aluminum alloys tested against steel balls using 15W40 and PILs are given in Figure 5 and Table 3, respectively. In the case of **PIL5**, it was not possible to detect the wear profile due to negligible wear loss and so the wear rate is not given in Table 3. As shown in Table 3, **PIL1**, **PIL2**, and **PIL3** showed higher wear rates than 15W40 engine oil. The increased wear rate can be related to insufficient lubrication, which induces the formation of junctions between the metal surfaces and causes adhesive and abrasive wear of the aluminum alloy. On the other hand, **PIL4** and **PIL5** exhibited much lower wear rates than 15W40, suggesting that lubricant molecules are adsorbed onto the metal surface to form a protective layer, which reduces the friction coefficient as shown in Figure 4, thereby reducing the wear loss.

Table 3. The wear rates of aluminum alloys tested against a steel ball under liquid lubrication.

Lubricant	15W40	PIL1	PIL2	PIL3	PIL4	PIL5
Wear rate ($mm^3\ N^{-1}\ m^{-1} \times 10^5$)	1.7	8.1	19.8	8.0	0.0085	ND

ND: Not detectable

3. Conclusions

PILs on the base of Edbea with formic, acetic, boric, decanoic, and gentisic acids were synthesized, respectively. All the PILs, except **PIL3** in creamy form, are liquid at room temperature. According to the elemental analysis results, PILs **1**–**3** are diprotonated with the nitrogen of amine, while PILs **4** and **5** are monoprotonated with the nitrogen of amine. Moreover, the quantum chemical calculations showed that two hydrogen bonds formed in CA-type ILs and four hydrogen bonds formed in CA_2-type ILs. The effect of the anion's alkyl chain length and the anion's aromatic type on the viscosity of PILs was determined. In the thermal decomposition mechanism of

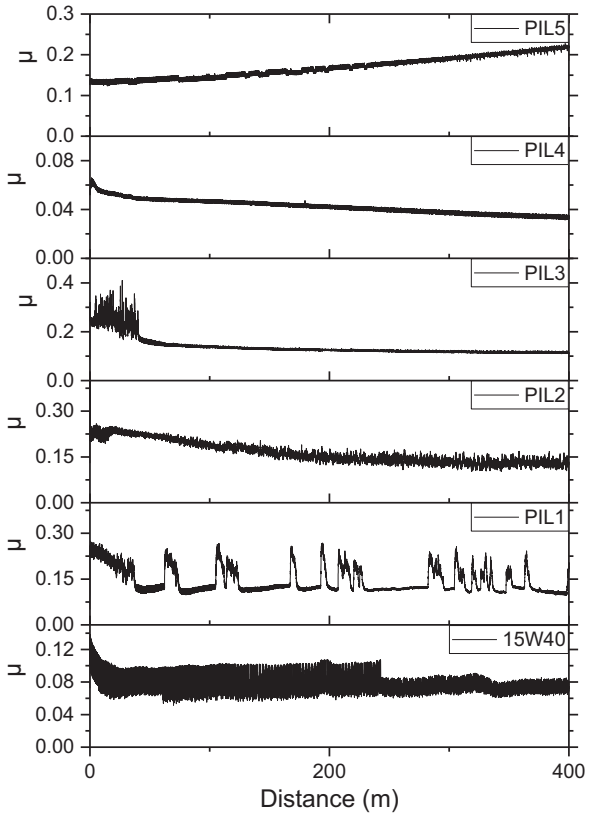

Figure 4. The mean values of coefficient of friction (COF) recorded during the sliding wear test.

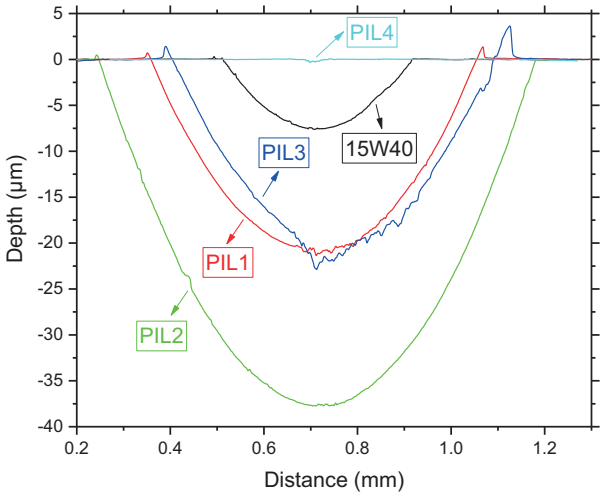

Figure 5. The wear profiles of aluminum alloys tested against steel balls using 15W40 engine oil and PILs.

PILs **1**–**5**, initially the acid anions decompose, and then the cation begins to decompose. It was also observed that **PIL4** and **PIL5** have better lubricating properties than 15W40 and the other PILs. **PIL1**, **PIL2**, and **PIL3** exhibited inadequate lubrication during the sliding wear test, causing an increased wear rate of the aluminum alloy.

4. Experimental

4.1. Materials

2,2′-(Ethylenedioxy)-bis(ethylamine) { Edbea} ($C_6H_{16}N_2O_2$), HCOOH, CH_3COOH, $B(OH)_3$, $CH_3(CH_2)_8COOH$, and $C_6H_5O_2COOH$ were purchased from Sigma-Aldrich and used without further purification.

4.2. Measurements

The FTIR spectra of PILs **1**–**5** were recorded on a Jasco FT/IR-430 spectrometer in KBr discs and reported in cm^{-1} units. ^1H, $^{13}C\{^1H\}$, and $^{31}P\{^1H\}$ NMR spectra were recorded on a Bruker DPX FT-NMR (600 MHz) spectrometer ($SiMe_4$ as an internal standard for ^1H), operating at 600 and 150 MHz. The spectrometer was equipped with a 5-mm PABBO BB inverse-gradient probe and the standard Bruker pulse program was used.[37] The TG and DTG curves were obtained using a PYRIS Diamond TG/DTA apparatus in a dynamic nitrogen atmosphere (heating rate: 10 °C/min, aluminum crucibles, mass ~10 mg, and temperature range 35–500 °C). The viscosities of PILs **1**, **2**, **4**, and **5** were measured using a Brookfield DV2TRVCP viscometer.

4.3. General procedure for the synthesis of PILs 1–5

A mixture of Edbea and formic acid, acetic acid, boric acid, decanoic acid, or gentisic acid is prepared in the molar ratio 1:1. Edbea is placed in a two-necked 100-mL round-bottomed flask fitted with a dropping funnel and connected to a condenser. Formic acid, acetic acid, boric acid, decanoic acid, or gentisic acid is placed in the dropping funnel and added dropwise to the Edbea in the flask. The reaction is vigorous, and the rate is controlled by regulating the acid addition. The reaction should be complete in about 24 h. The product should be viscose liquid. The most probable formation reactions of PILs **1**–**5** are illustrated in the Scheme.

4.3.1. Synthesis of compound PIL1

Anal. Calc. for $C_6H_{17}N_2O_2^+(CHO_2^-)_2.5H_2O$ (%): C, 29.09; H, 9.15; N, 8.48 Found (%): C, 29.62; H, 8.71; N, 8.59. FTIR (KBr, cm^{-1}): ν 2969 (C–H aliph. asymm.), 2880 (C–H aliph. symm.), 2703 (NH^+), 1587, 1487 (COO^-), 1105 (C–N). ^1H NMR (DMSO, ppm, numberings of protons are given in the Scheme): 2.73 (s, 2H, $\boldsymbol{H_1}$), 3.50 (s, 2H, $\boldsymbol{H_2}$), 3.43 (s, 4H, $\boldsymbol{H_3}$), 4.33 (s, 2H, $\boldsymbol{H_4}$), 3.22 (s, 2H, $\boldsymbol{H_5}$), 5.51 (s, 2H, $N\boldsymbol{H_2}$), 7.99 (s, 2H, $^+N\boldsymbol{H_3}$), 8.44 (s, 1H, $\boldsymbol{H_6}$). ^{13}C NMR (DMSO, ppm, numberings of carbons are given in the Scheme): 40.32 ($\mathbf{C_1}$), 70.97 ($\boldsymbol{C_2}$), 69.72 ($\mathbf{C_3}$), 167.11 ($\boldsymbol{C}$=O).

4.3.2. Synthesis of compound PIL2

Anal. Calc. for $C_6H_{17}N_2O_2^+(C_2H_3O_2^-)_2.5H_2O$ (%): C, 33.51; H, 9.56; N, 7.82 Found (%): C, 32.77; H, 8.19; N, 8.12. FTIR (KBr, cm^{-1}): ν 2925 (C–H aliph. asymm.), 2880 (C–H aliph. symm.), 2697 (NH^+), 1568, 1491 (COO^-), 1106 (C–N). ^1H NMR (DMSO, ppm, numberings of protons are given in the Scheme): 2.76 (t, $^3J_{HH}$ 4.5 Hz, 2H, $\boldsymbol{H_1}$), 3.50 (t, $^3J_{HH}$ 4.6 Hz, 2H, $\boldsymbol{H_2}$), 3.47 (s, 4H, $\boldsymbol{H_3}$), 5.17 (s, 2H, $\boldsymbol{H_4}$), 3.02 (s, 2H, $\boldsymbol{H_5}$), 5.17 (s, 2H, $N\boldsymbol{H_2}$), 7.98 (s, 2H, $^+N\boldsymbol{H_3}$), 1.68 (s, 1H, $\boldsymbol{H_6}$). ^{13}C NMR (DMSO, ppm, numberings of carbons are given in the Scheme): 39.87 ($\mathbf{C_1}$), 70.06 ($\boldsymbol{C_2}$), 69.81 ($\mathbf{C_3}$), 24.90 ($\mathbf{C_4}$), 176.22 ($\boldsymbol{C}$=O).

4.3.3. Synthesis of compound PIL3

Anal. Calc. for $C_6H_{17}N_2O_2^+(BH_2O_3^-)_2.C_2H_5OH$ (%): C, 30.22; H, 8.88; N, 8.81 Found (%): C, 29.98; H, 7.26; N, 9.61. FTIR (KBr, cm^{-1}): ν 3423 (O–H), 2912 (C–H aliph. asymm.), 2875 (C–H aliph. symm.), 2703 (NH^+), 1323 (B–O), 1105 (C–N). ^{1}H NMR (DMSO, ppm, numberings of protons are given in the Scheme): 2.71 (s, 2H, $\boldsymbol{H_1}$), 3.50 (s, 2H, $\boldsymbol{H_2}$), 3.41 (s, 4H, $\boldsymbol{H_3}$), 4.23 (s, 2H, $\boldsymbol{H_4}$), 3.04 (s, 2H, $\boldsymbol{H_5}$), 5.66 (s, 2H, N$\boldsymbol{H_2}$), 7.99 (s, 2H, $^+$N$\boldsymbol{H_3}$). ^{13}C NMR (DMSO, ppm, numberings of carbons are given in the Scheme): 40.61 ($\mathbf{C_1}$), 71.47 ($\boldsymbol{C_2}$), 69.65 ($\mathbf{C_3}$).

4.3.4. Synthesis of compound PIL4

Anal. Calc. for $C_6H_{17}N_2O_2^+(C_{10}H_{19}O_2^-).3H_2O$ (%): C, 51.31; H, 11.30; N, 7.48 Found (%): C, 51.34; H, 9.76; N, 7.26. FTIR (KBr, cm^{-1}): ν 2925 (C–H aliph. asymm.), 2856 (C–H aliph. symm.), 2703 (NH^+), 1565, 1473 (COO^-), 1115 (C–N). ^{1}H NMR (DMSO, ppm, numberings of protons are given in the Scheme): 2.71 (s, 2H, $\boldsymbol{H_1}$), 3.51 (s, 2H, $\boldsymbol{H_2}$), 3.42 (s, 4H, $\boldsymbol{H_3}$), 4.31 (s, 2H, $\boldsymbol{H_4}$), 3.05 (s, 2H, $\boldsymbol{H_5}$), 6.62 (s, 2H, N$\boldsymbol{H_2}$), 8.33 (s, 2H, $^+$N$\boldsymbol{H_3}$), 2.04 (s, 2H, $\boldsymbol{H_a}$), 1.96 (s, 2H, $\boldsymbol{H_b}$), 1.42 (s, 10H, $\boldsymbol{H_c}$), 1.23 (s, 2H, $\boldsymbol{H_d}$), 0.85 (s, 3H, $\boldsymbol{H_e}$). ^{13}C NMR (DMSO, ppm, numberings of carbons are given in the Scheme) 40.36 ($\mathbf{C_1}$), 71.21 ($\boldsymbol{C_2}$), 69.57 ($\mathbf{C_3}$), 176.95 ($\boldsymbol{C}$=O), 36.96 ($\boldsymbol{C_a}$), 31.36 ($\boldsymbol{C_f}$), 29.21 ($\boldsymbol{C_e}$), 29.09 ($\boldsymbol{C_d}$), 28.78 ($\boldsymbol{C_c}$), 25.88 ($\boldsymbol{C_b}$), 22.14 ($\boldsymbol{C_g}$), 13.94 ($\boldsymbol{C_h}$).

4.3.5. Synthesis of compound PIL5

Anal. Calc. for $C_6H_{17}N_2O_2^+(C_7H_5O_4^-).5H_2O$ (%): C, 46.15; H, 7.75; N, 8.28 Found (%): C, 45.88; H, 6.36; N, 7.91. FTIR (KBr, cm^{-1}): ν 3446 (O–H), 3033 (C–H arom), ν 2915 (C–H aliph. asymm.), 2879 (C–H aliph. symm.), 2700 (NH^+), 1574, 1488 (COO^-), 1126 (C–N). ^{1}H NMR (DMSO, ppm, numberings of protons are given in the Scheme): 2.83 (t, $^3J_{HH}$ 4.9 Hz, 2H, $\boldsymbol{H_1}$), 3.50 (t, $^3J_{HH}$ 4.7 Hz, 2H, $\boldsymbol{H_2}$), 3.17 (s, 4H, $\boldsymbol{H_3}$), 3.53 (s, 2H, $\boldsymbol{H_4}$), 2.95 (t, $^3J_{HH}$ 5.0 Hz, 2H, $\boldsymbol{H_5}$), 5.25 (s, 2H, N$\boldsymbol{H_2}$), 8.01 (s, 2H, $^+$N$\boldsymbol{H_3}$), 6.49 (m, 1H, $\boldsymbol{H_a}$), 6.65 (dd, 1H, $\boldsymbol{H_b}$), 7.15 (d, 1H, $\boldsymbol{H_c}$). ^{13}C NMR (DMSO, ppm, numberings of carbons are given in the Scheme): 48.64 ($\mathbf{C_1}$), 69.71 ($\boldsymbol{C_2}$), 69.55 ($\mathbf{C_3}$), 172.40 ($\boldsymbol{C}$=O), 115.76 ($\boldsymbol{C_a}$), 154.56 ($\boldsymbol{C_b}$), 120.01 ($\boldsymbol{C_c}$), 120.09 ($\boldsymbol{C_d}$), 147.94 ($\boldsymbol{C_e}$), 119.25 ($\boldsymbol{C_f}$).

4.4. Computational process

Firstly, schematic structures of cations (C) { $[EdbeaH]^+$, $[EdbeaH_2]^{2+}$ } and anions (A) { $[HCOO]^-$, $[CH_3COO]^-$, $[H_2BO_3]^-$, $[CH_3(CH_2)_8COO]^-$, $[C_6H_3(OH)_2COO]^-$ } were modeled in the program GaussView 5.0.[38] Each ion was optimized in the program Gaussian 09, Revision D.01[39] at M062X/6-311+G(d,p) level[40] and imaginary frequencies were not observed in the vibrational frequency analysis of ions. Then the PILs of CA and CA_2 types were also optimized at the given level. Two imaginary frequencies were observed in the optimization of CA-type ILs and four were observed in CA_2-type optimization. This is expected. Because the ionic interaction is not directional, the stationary point cannot be found. Reaction energies of the type $C^+ + A^- \rightarrow CA$ and $C^{2+} + A^- \rightarrow CA_2$ reactions were calculated from the total energy values of ions and PILs, where CA and CA_2 are the PILs that are not stationary points.

The same studies were also carried out at M062X/6-311++G(d,p) level. We could not obtain a significant

difference between M062X/6-311+G(d,p) and M062X/6-311++G(d,p) levels. Therefore, we did not use the results computed at M062X/6-311++G(d,p) level. M062X/6-311++G(d,p) level adds diffuse functions to the hydrogen atoms. Diffuse functions on the hydrogen atoms seldom make a significant difference in accuracy.[20]

4.5. Tribological studies

4.6. Specimen preparation

An AA7075 round bar with a diameter of 25 mm was cut into 10-mm sections using a SiC-precision cut-off wheel. Disc specimens were ground flat on 240, 400, 800, 1200, and 2000 grit SiC emery papers consecutively. Then polishing was applied using 3-µm diamond paste in an alcohol-based lubricant and subsequently using 50 nm of colloidal silica suspension to obtain a mirror-like surface finish. After metallographic specimen preparation, disc specimens were ultrasonically cleaned in acetone for 2 min and subsequently in methanol for 2 min.

4.6.1. Friction and wear test

A CSM Instruments standard tribometer was used in the linear reciprocating wear test at room temperature (23 ± 2 °C) under liquid lubrication. The wear tests were conducted at a normal load of 3 N and a constant sliding velocity of 0.06 m s^{-1}. The stroke length and the total sliding distance were 10 mm and 400 m, respectively. A 100Cr6 steel ball 6 mm in diameter was used as the counter body in the wear test. Five drops of lubricant were applied to the aluminum alloy surface prior to each test and no additional lubricant was supplied during the test. 15W40 commercial engine oil was used in this study for comparison of its frictional and wear properties with those of PILs. After the wear test, the material volume loss was estimated from the wear track profile, which was obtained by an Ambios xp-2 high resolution stylus profilometer.

References

1. Karadağ, A.; Destegül, A. *J. Mol. Liq.* **2013**, *177*, 369-375.
2. Thawarkar, S.; Khupse, N. D.; Kumar, A. *Chem. Phys. Chem.* **2016**, *17*, 1006-1017.
3. Ghandi, K. *Green and Sustainable Chemistry* **2014**, *4*, 44-53.
4. Greaves, T. L.; Drummond, C. J. *Chem. Rev.* **2008**, *108*, 206-237.
5. Hayes, R.; Imberti, S.; Warr, G. G.; Atkin, R. *Angew. Chem. Int. Ed.* **2013**, *52*, 4623-4627.
6. Korkmazer, E. *MSc. Gaziosmanpasa University, Turkey*, 2017.
7. Angell, C. A.; Ansari, Y.; Zhao, Z. *Faraday Discuss.* **2012**, *154*, 9-27.
8. Gabriel, S.; Weiner, J. *Eur. J. Inorg. Chem.* **1888**, 2669-2679.
9. Evans, D. F.; Yamauchi, A.; Roman, R.; Casassa, E. Z. *J. Colloid Interface Sci.* **1982**, *88*, 89-89.
10. Welton, T. *Coord. Chem. Rev.* **2004**, *248*, 2459-2477.
11. Vissera, A. E.; Swatloski, R. P.; Reichert, W. M.; Mayton, R.; Sheff, S.; Wierzbicki, A.; Davis, J. H.; Rogers, R. D. *Chem. Commun.* **2001**, 135-136.
12. Mizuuchi, H.; Jaitely, V.; Murdan, S.; Florence, A. T. *Eur. J. Pharm. Sci.* **2008**, *33*, 326-331.
13. Hagiwara, R.; Lee, J. S. *Electrochem.* **2007**, *75*, 23-34.
14. Ma, J.; Hong, X. *J. Env. Manag.* **2012**, *99*, 104-109.
15. Akbaş, H.; Okumuş, A.; Karadağ, A.; Kılıç, Z.; Hökelek, T.; Koç, L. Y.; Açık, L.; Aydın, B.; Türk, M. *J. Therm. Anal. Calorim.* **2016**, *123*, 1627-1641.

16. Elmas, G.; Okumuş, A.; Kılıç, Z.; Gönder, L. Y.; Açık, L.; Hökelek, T. *Journal of the Turkish Chemical Society, Section A: Chemistry* **2016**, *3*, 25-46.
17. Akbaş, H.; Karadağ, A.; Aydın, A.; Destegül, A.; Kılıç, Z. *J. Mol. Liq.* **2017**, *230*, 482-495.
18. Okumuş, A.; Akbaş, H.; Karadağ, A.; Aydın, A.; Kılıç, Z.; Hökelek, T. *Chem. Select.* **2017**, *2*, 4988-4999.
19. Elmas, G.; Okumuş, A.; Kılıç, Z.; Çelik, S. P.; Açık, L. *Journal of the Turkish Chemical Society, Section A: Chemistry* **2017**, *4*, 993-1016.
20. Foresman, J. B.; Frisch, ?. *Exploring Chemistry with Electronic Structure Methods*; 2nd ed., Gaussian Inc.: Pittsburgh, PA, USA, 1996.
21. Karakaş, D. *Turkish Computational and Theoretical Chemistry* **2017**, *1*, 1-10.
22. Sayın, K.; Karakaş, D. *Turkish Computational and Theoretical Chemistry* **2017**, *1*, 11-16.
23. Kariper, S. E.; Sayın, K.; Karakaş, D. *J. Mol. Struc.* **2017**, *1149*, 473-486.
24. Sayın, K.; Karakaş, D. *Spectrochim. Acta Part A: Mol. Biomol. Spect.* **2018**, *188*, 537-546.
25. Zhou, F.; Liang, Y.; Liu, W. *Chem. Soc. Rev.* **2009**, *38*, 2590-2599.
26. González, R.; Bartolomé, M.; Blanco, D.; Viesca, J. L.; Fernández-González, A.; Battez, A. H. *Trib. Int.* **2016**, *98*, 82-93.
27. Qu, J.; Bansal, D. G.; Yu, B.; Howe, J. Y.; Luo, H.; Dai, S.; Li, H.; Blau, P. J.; Bunting, B. G.; Mordukhovich, G.; et al. *ACS Appl. Mater. Interfaces* **2012**, *4*, 997-1002.
28. Mu, Z.; Liu, W.; Zhang, S.; Zhou, F. *Chem. Lett.* **2004**, *33*, 524-525.
29. Mu, Z.; Zhou, F.; Zhang, S.; Liang, Y.; Liu, W. *Trib. Int.* **2005**, *38*, 725-731.
30. Jiménez, A. E.; Bermúdez, M. D.; Iglesias, P.; Carrión, F. J.; Martínez-Nicolás, G. *Wear* **2006**, *260*, 766-782.
31. Jiménez, A. E.; Bermúdez, M. D.; Carrión, F. J.; Martínez-Nicolás, G. *Wear* **2006**, *261*, 347-359.
32. Liu, X.; Zhou, F.; Liang, Y.; Liu, W. *Wear* **2006**, *261*, 1174-1179.
33. Jiménez, A. E.; Bermúdez, M. D. *Trib. Letts.* **2007**, *26*, 53-60.
34. Mu, Z.; Wang, X.; Zhang, S.; Liang, Y.; Bao, M.; Liu, W. *J. Trib.* **2008**, *130*, 034501-034505.
35. Jiménez, A. E.; Bermúdez, M. D. *Wear* **2008**, *265*, 787-798.
36. Landolt, D. *J. Phys. D: Appl. Phys.* **2006**, *39*, 3121.
37. Bruker program 1D WIN-NMR (release 6.0) and 2D WIN-NMR (Release 6.1).
38. Dennington, R.; Keith, T.; Millam, J. GaussView Version 5 Semichem Inc. Shawnee Mission, KS, USA, 2009.
39. Frisch, M. J.; Trucks, G. W.; Schlegel, H. B.; Scuseria, G. E.; Robb, M. A.; Cheeseman, J. R.; Scalmani, G.; Barone, V.; Mennucci, B.; Petersson, G. A.; et al. Gaussian 09 Revision A.02 Gaussian Inc. Wallingford, CT, USA, 2009.
40. Zhao, Y.; Truhlar, D. G. *Theor. Chem. Acc.* **2008**, *120*, 215-241.

Supplementary

Table S1. Thermoanalytical data of PILs **(1-5)**.

Compound	Stage	Temperature range; °C	DTG(max)/°C	Mass loss (Obs.)/Δm %	Total mass loss (Obs.)/Δm %
PIL1	1	25-140	66	26.48	26.48
	2	140-253	161	26.63	53.11
$C_8H_{30}N_2O_{11}$ 330,33 $gmol^{-1}$	3	253-369	294	45.96	99.07
PIL2	1	30-117	89	24.40	24.40
	2	117-167	174	33.11	57.51
$C_{10}H_{34}N_2O_{11}$ 358,39 $gmol^{-1}$	3	167-294	220	40.60	98.11
PIL3	1	32-101	116	14.10	14.10
	2	101-191	162	31.87	45.97
$C_8H_{28}B_2N_2O_9$ 317,94 $gmol^{-1}$	3	191-439	226	38.33	84.30
PIL4	1	30-124	66	14.65	14.65
	2	124-235	188	46.17	60.82
$C_{16}H_{42}N_2O_7$ 374,52 $gmol^{-1}$	3	235-470	343	39.00	99.82
PIL5	1	30-213	139	22.86	22.86
$C_{13}H_{26}N_2O_8$ 392,43 $gmol^{-1}$	2	213-420	241	70.92	93.78

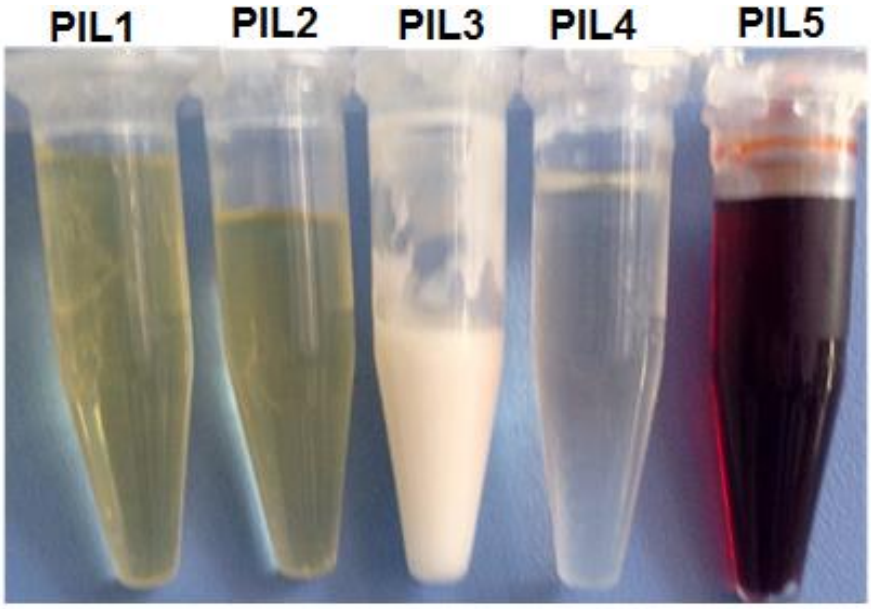

Figure S1. The states of **PILs (1-5)**.

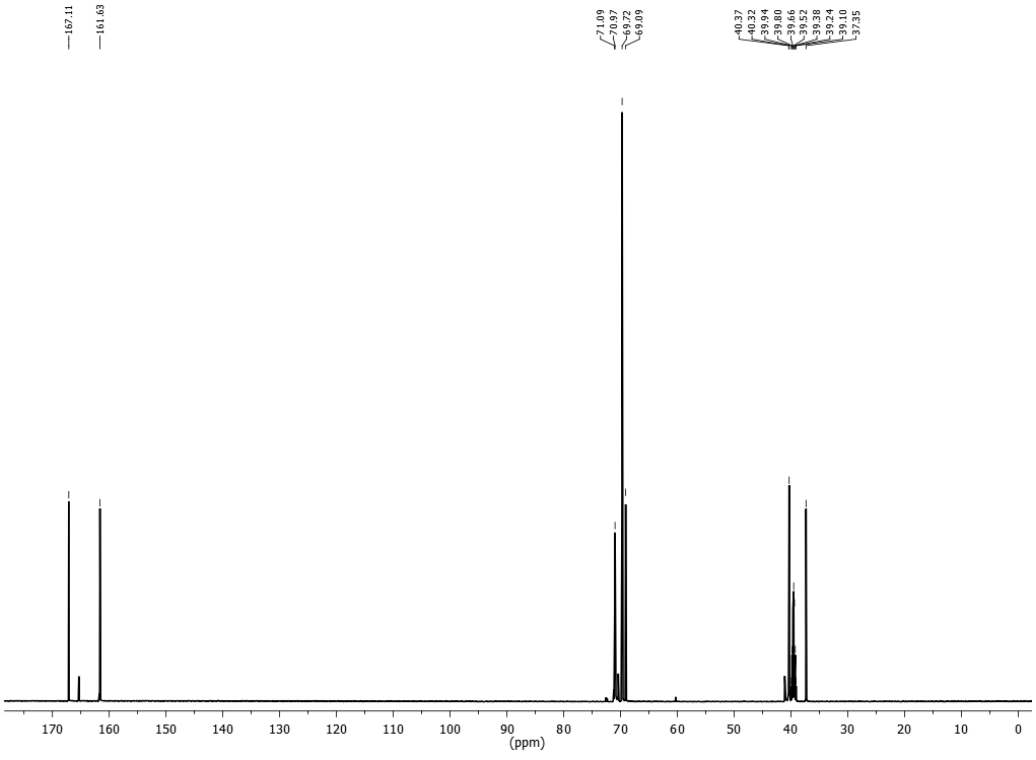

Figure S2. The ^{13}C NMR spectra of **PIL1**.

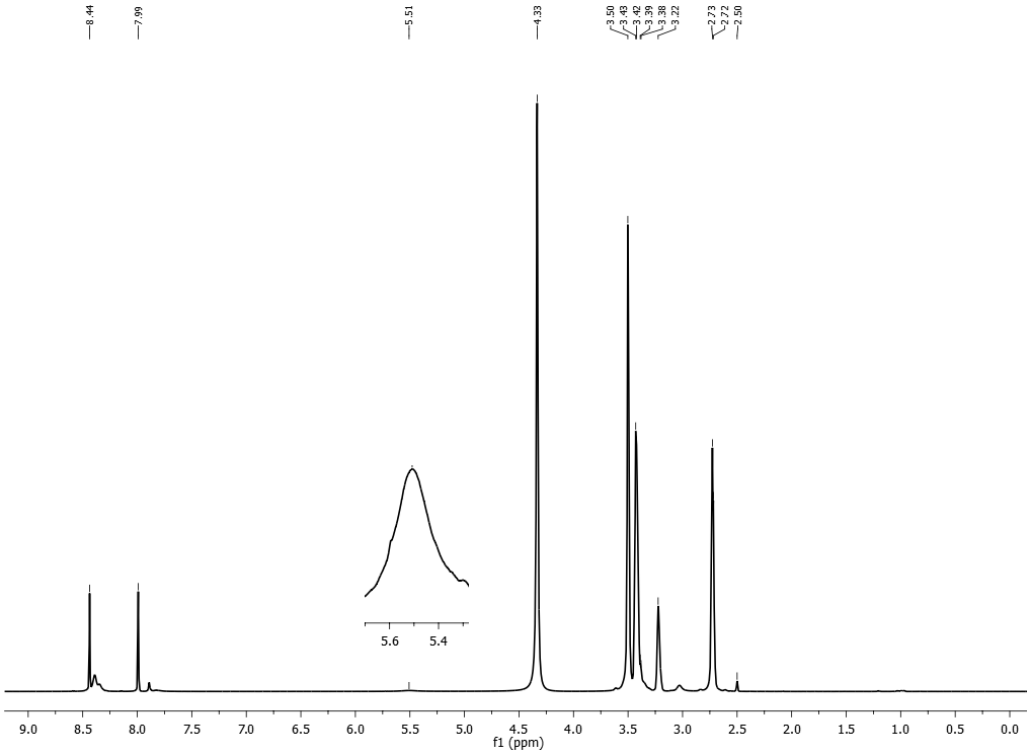

Figure S3. The ^{1}H NMR spectra of **PIL1**.

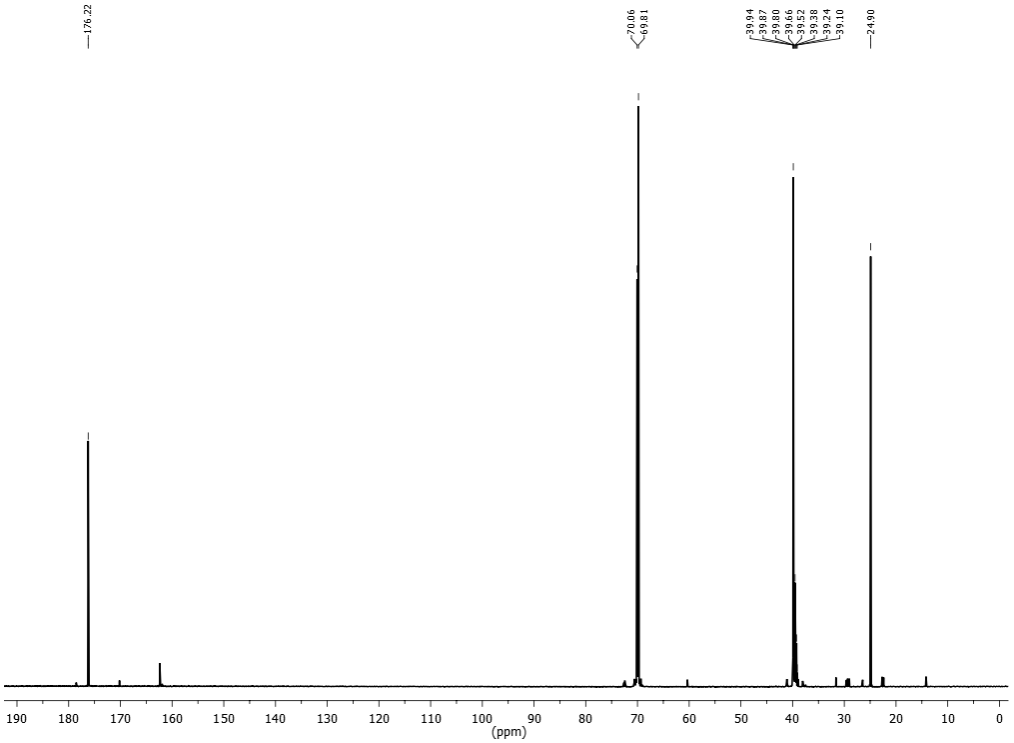

Figure S4. The ^{13}C NMR spectra of **PIL2**.

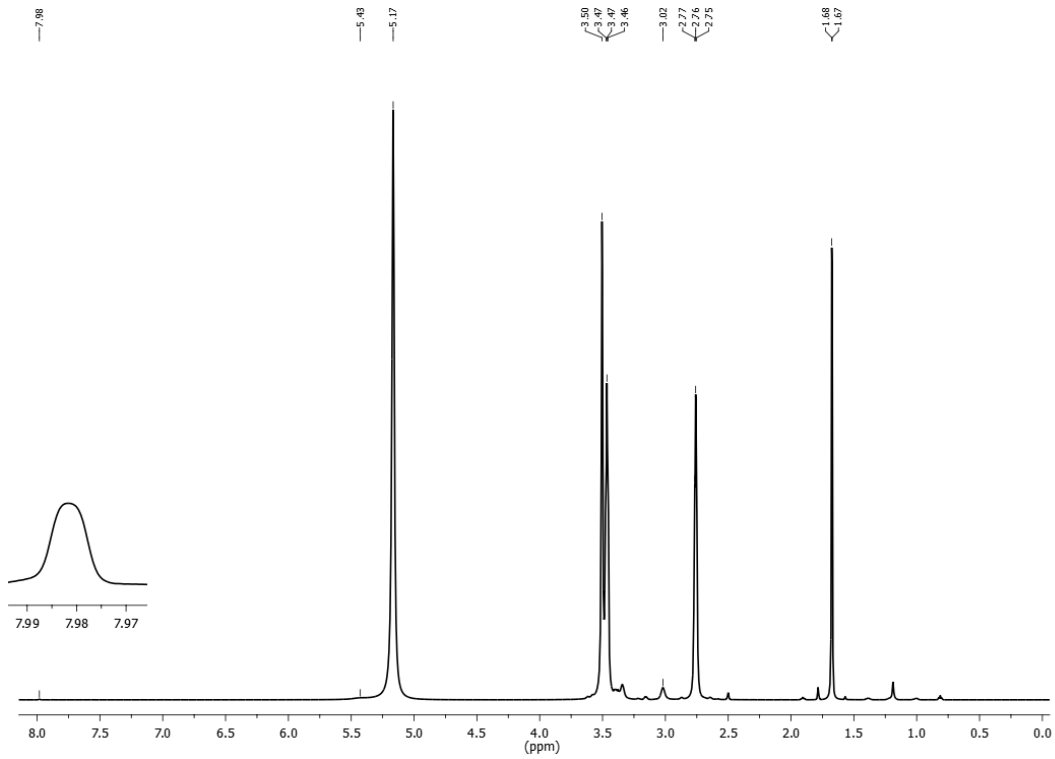

Figure S5. The ^{1}H NMR spectra of **PIL2**.

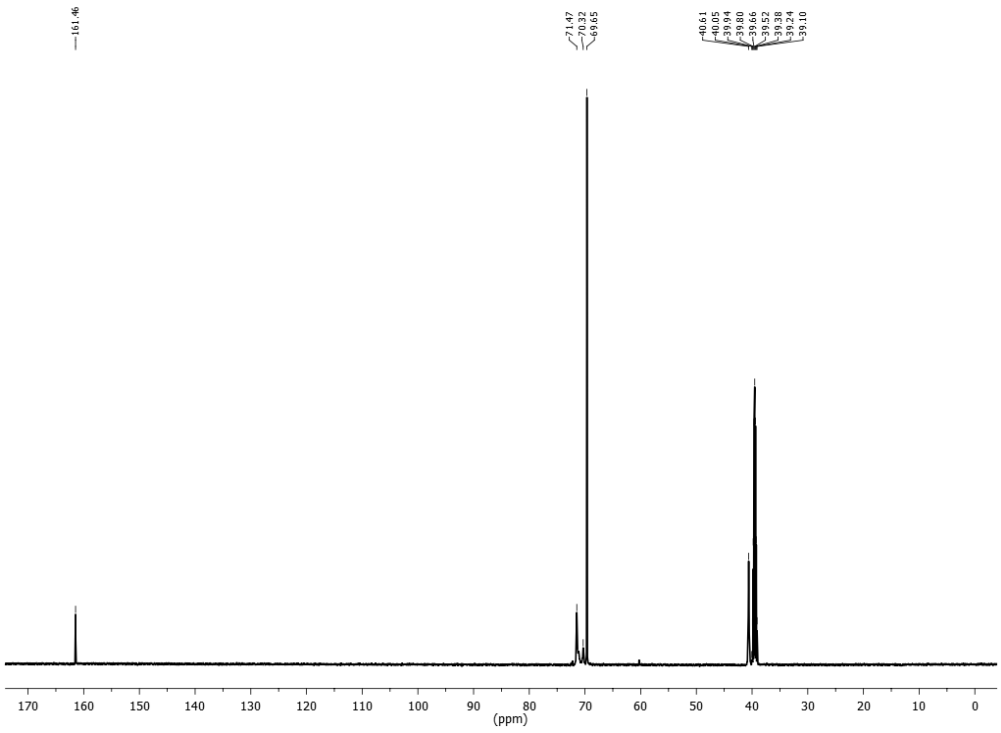

Figure S6. The ^{13}C NMR spectra of **PIL3**.

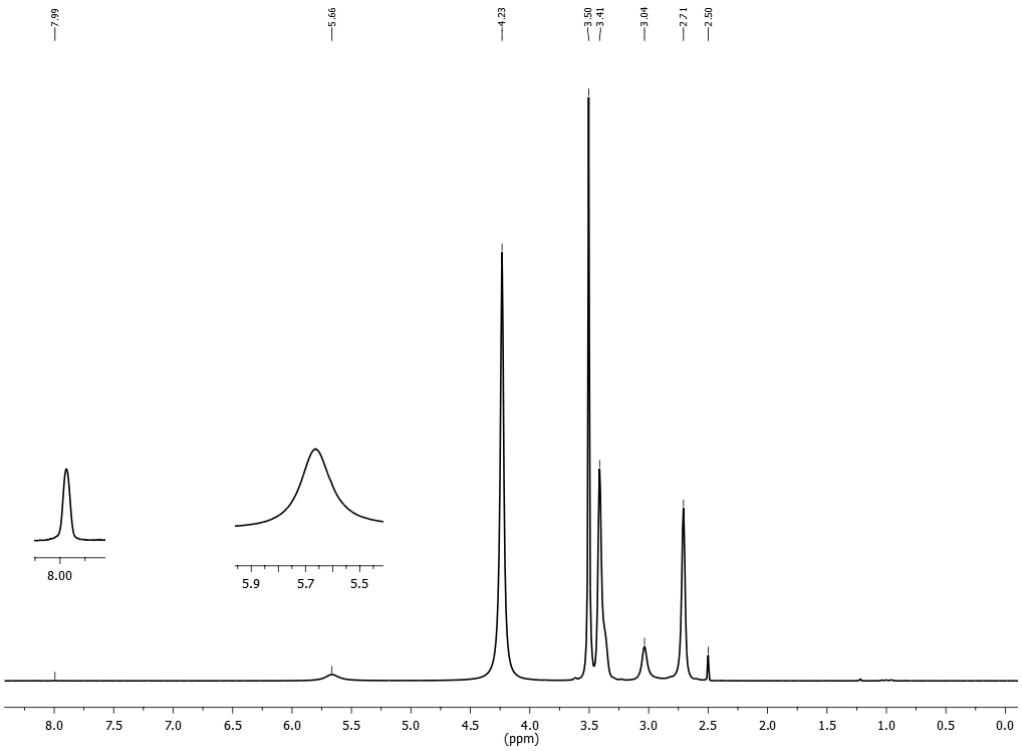

Figure S7. The ^{1}H NMR spectra of **PIL3**.

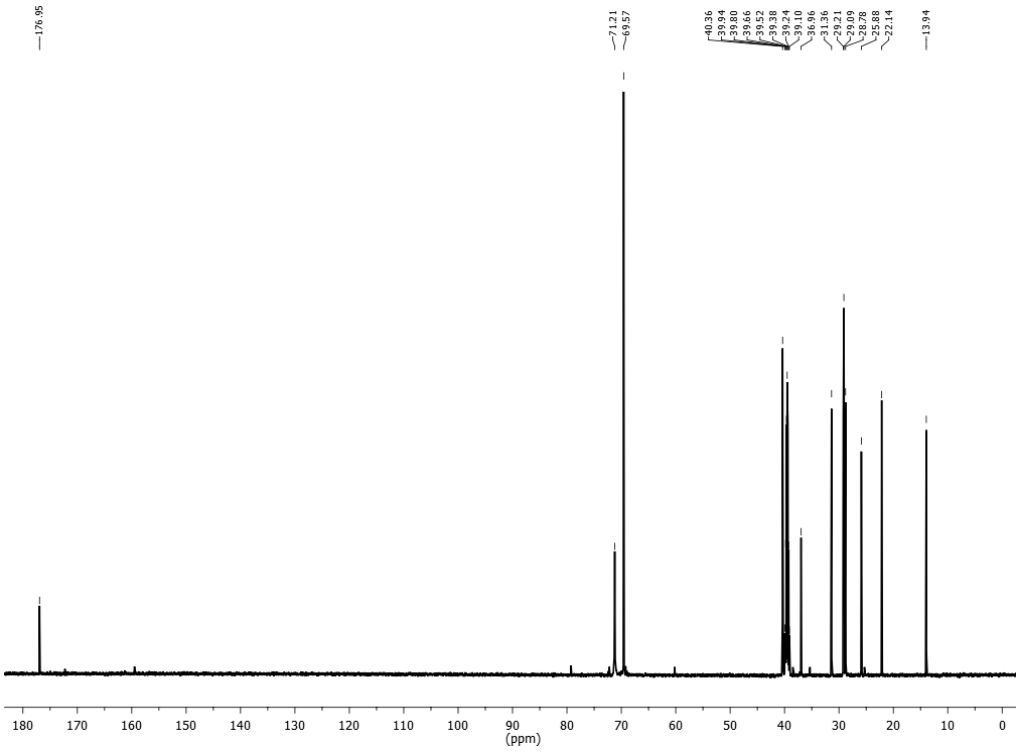

Figure S8. The ^{13}C NMR spectra of **PIL4**.

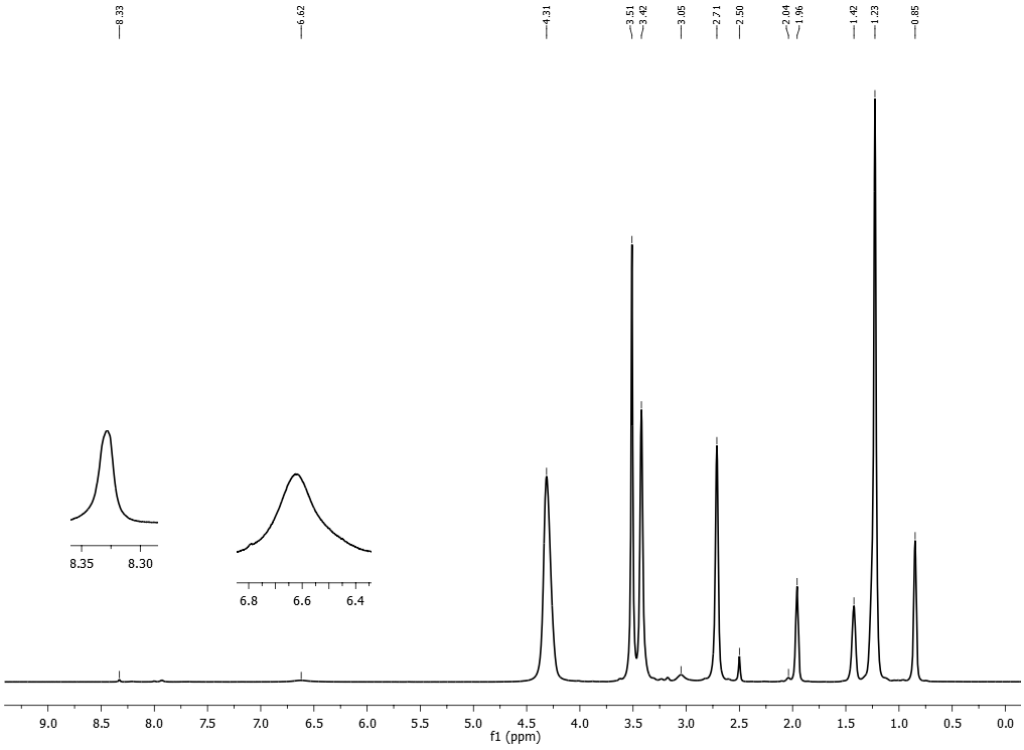

Figure S9. The ^{1}H NMR spectra of **PIL4**.

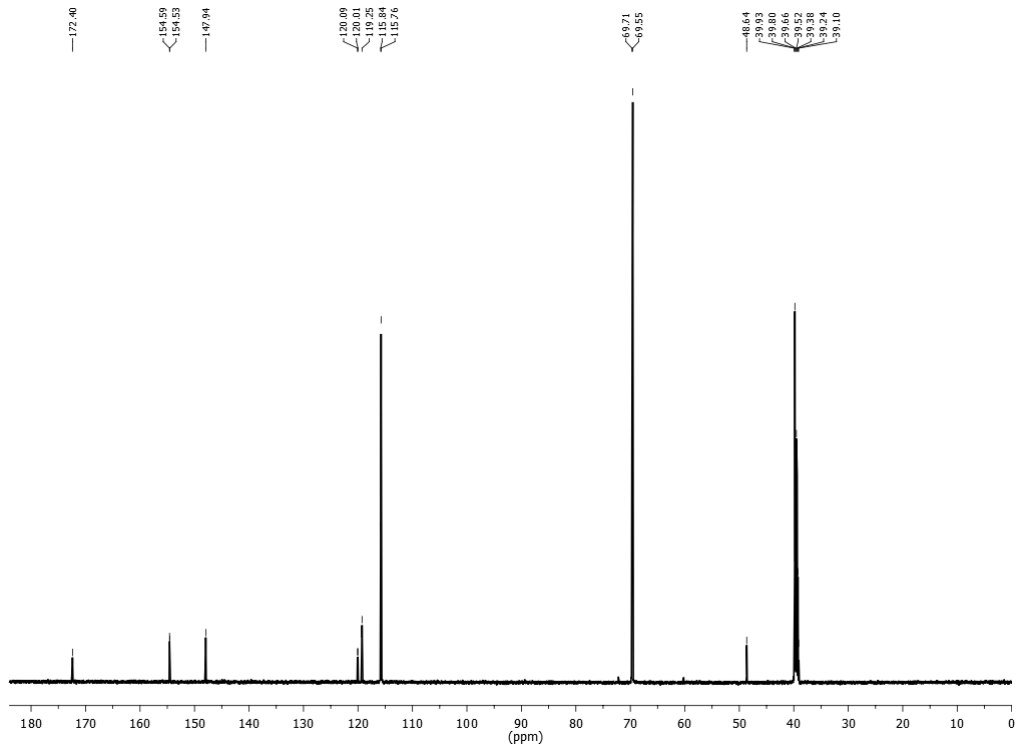

Figure S10. The ^{13}C NMR spectra of **PIL5**.

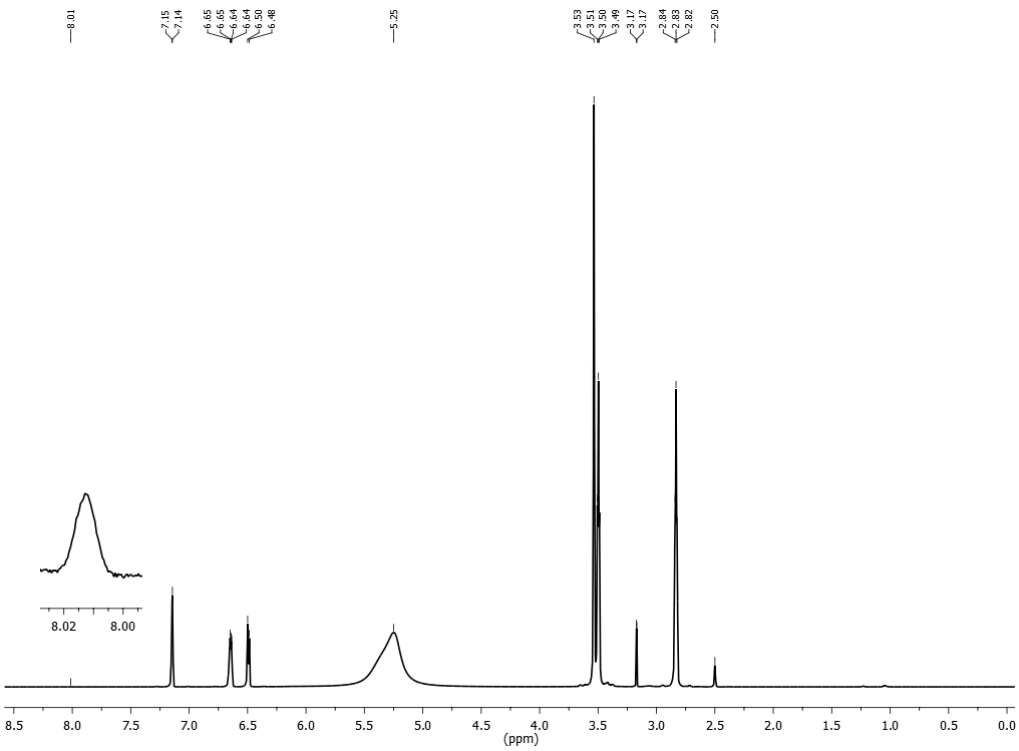

Figure S11. The ^{1}H NMR spectra of **PIL5**.

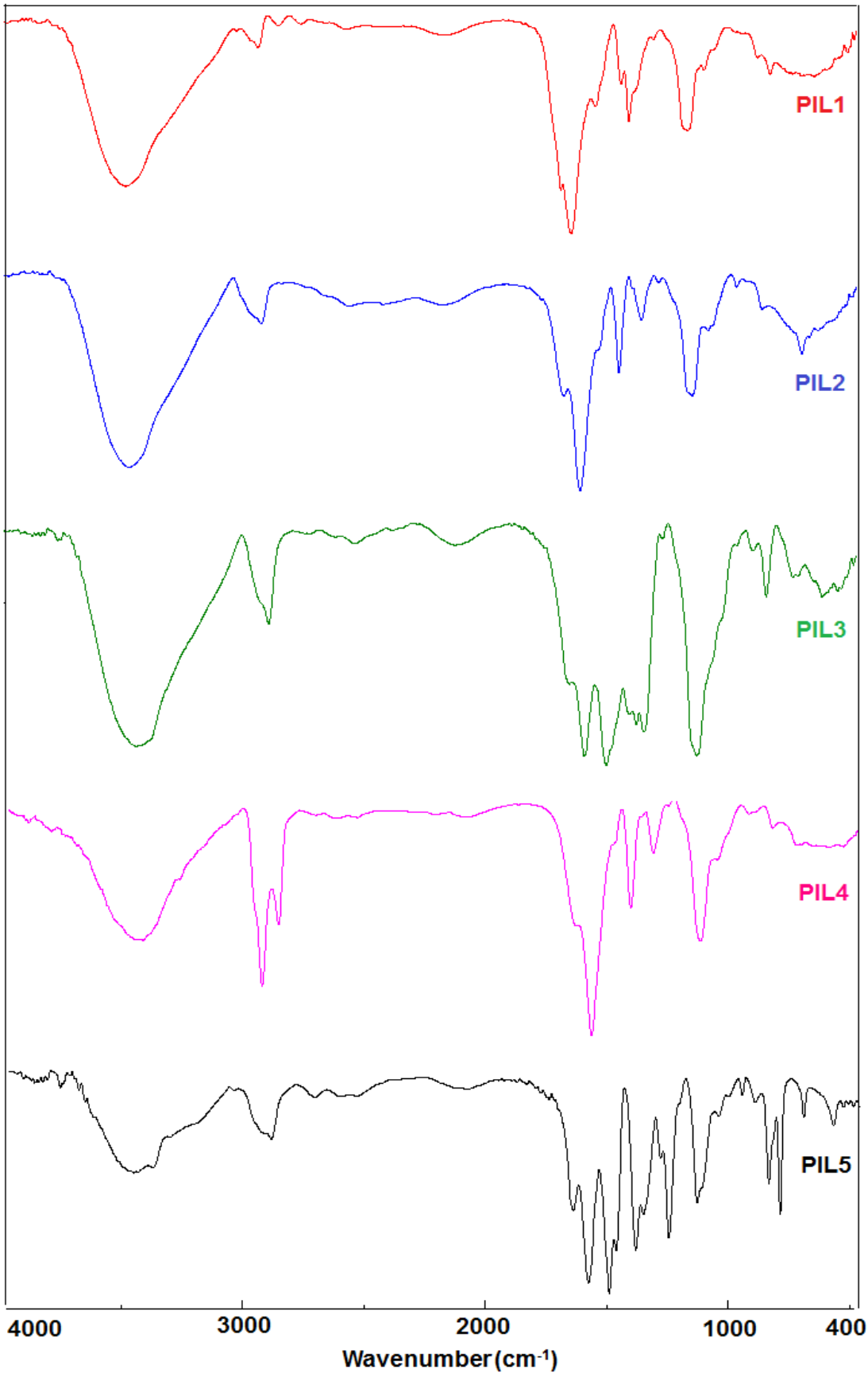

Figure S12. IR spectra of **PILs (1-5)**.

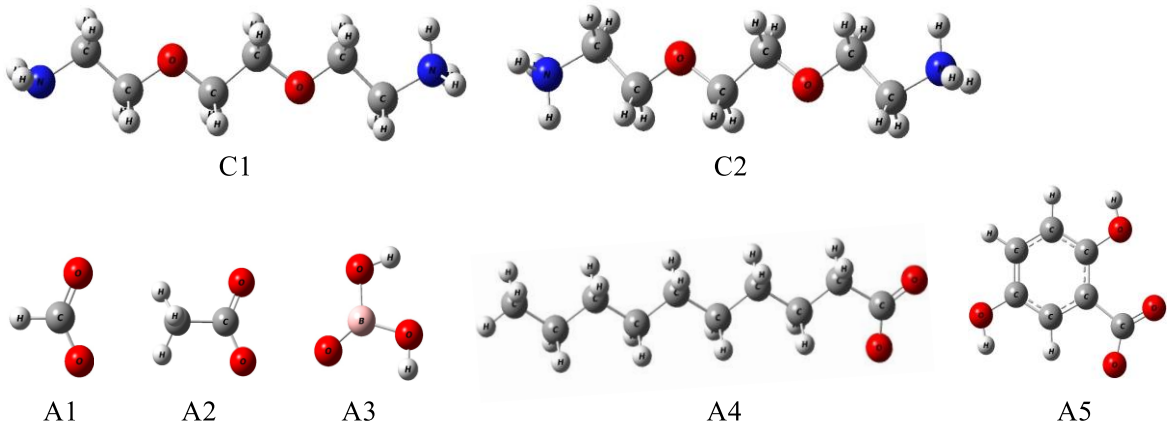

Figure S13. Optimized structures of cations (C1 and C2) and anions (A1, A2, A3, A4 and A5) obtained at the M062X/6-311+G(d,p) level in gas phase. C1=$[EdbeaH]^{+}$, C2=$[EdbeaH_2]^{2+}$, A1=$[HCOO]^{-}$, A2=$[CH_3COO]^{-}$, A3=$[H_2BO_3]^{-}$, A4=$[CH_3(CH_2)_8COO]^{-}$, A5=$[C_6H_3(OH)_2COO]^{-}$.

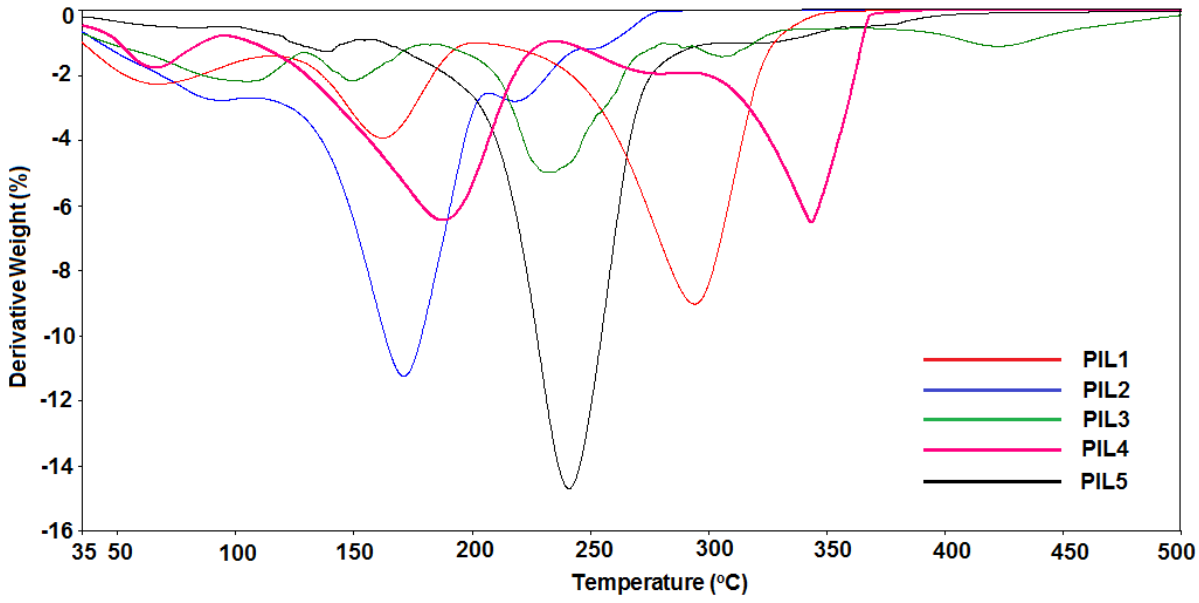

Figure S14. DTG curves of **PILs (1-5)**.